IET Radar Sonar and Navigation, Volume 10, Issue 8, 2016, pp. 1400-1410
DOI:10.1049/iet-rsn.2015.0474

EXPERIMENTAL ANALYSIS OF MULTISTATIC MULTIBAND RADAR SIGNATURES OF WIND TURBINES

Francesco Fioranelli[1], Matthew Ritchie[1], Alessio Balleri[2], Hugh Griffiths[1]

1 Department of Electronic and Electrical Engineering, University College London, London, UK
2 Centre for Electronic Warfare, Cranfield University, Defence Academy of the United Kingdom, Shrivenham, UK

Abstract

This paper presents the analysis of recent experimental data acquired using two radar systems at S-band and X-band to measure simultaneous monostatic and bistatic signatures of operational wind turbines near Shrivenham, UK. Bistatic and multistatic radars are a potential approach to mitigate the adverse effects of wind farm clutter on the performance of radar systems, which is a well-known problem for Air Traffic Control and Air Defence radar. This analysis compares the simultaneous monostatic and bistatic micro-Doppler signatures of two operational turbines and investigates the key differences at bistatic angles up to 23°. The variations of the signature with different polarisations, namely VV and HH, are also discussed.

1. Introduction

The generation of electricity from renewable and environmental-friendly sources is a key priority of the United Kingdom and many other countries in order to reduce the dependence on fossil fuels and the production of greenhouse gases. Onshore and offshore wind energy is expected to greatly contribute towards the goal of generating 15% of energy from renewable sources by 2020 which the UK Government has set [1]. RenewableUK, the UK leading renewable energy trade association, has estimated that at the end of 2014 around 17 TWh (Terawatt-hours) of electricity were generated annually by the total onshore installed capacity in the UK, equivalent to the consumption in excess of 4 million households [2]. It is also reported that a single 2.5 MW turbine can generate enough electricity to power 1400 households in a year, and this is equivalent to running an average computer for over 2000 years or making 230 million cups of tea [2].

However, it is well known that wind turbines and wind farms can have a detrimental effect on the performance of radar systems, in particular those used for Air Traffic Control (ATC) to provide services to civilian aircraft and manage their traffic, and for Air Defence (AD) to detect and localise possible unauthorised and hostile aircraft. As a result, the development of wind turbines and wind farms at many suitable sites across the UK is delayed or completely blocked because of objections

raised by military and civilian bodies. It is reported that more than half of wind farm developments in the UK have faced objections from the aviation sector and from the Ministry of Defence (MoD), and that objections due to radar issues accounted for approximately 12 GW of electricity generation capacity in 2013 [3-4]. The effects of wind farms on radar systems that are located within the line of sight of the radar include the increase of undesired returns that may generate false alarms, the reduction of probability of target detection in the area above and around wind farms (desensitisation of the radar), and the consequent loss of plotting and tracking capabilities in the affected area [5]. This is related to the large radar cross section (RCS) of the turbines (as much as 55 dBsm of peak RCS) in comparison with typical air targets (e.g. around 0-10 dBsm for a small fighter jet), as well as to the Doppler shifts created by the fast-moving tips of the turbine blades which can be comparable to those generated by slow moving air targets such as helicopters, landing commercial aircrafts, and small aircrafts [5].

Different mitigation techniques have been proposed to cope with the aforementioned effects. A good summary of such techniques can be found in [6] and in the document "Policy and Guidelines on Wind Turbines" issued by the UK Civil Aviation Authority (CAA) [7]. These techniques include actions on the wind farm design, such as relocation, terrain screening, rearranging the position of the turbines to minimize their effect on radar systems, reduction of the height of the turbines, reshaping of turbine parts to avoid specular radar reflections, and use of radar absorbing materials (RAM) to reduce the overall RCS. These techniques can be effective, but their suitability must be balanced with related additional costs for the wind farm development and with the possible reduction of the electrical capacity of the farm. Other mitigation techniques aim at improving the radar affected by the turbine, for instance adapting antenna beams, tilt, and side-lobes to minimize the return from wind farms, improving the detection and tracking algorithms to filter out the negative effect of wind farms, or using a multiple sensor approach with an "in-fill radar" that complements the coverage of the primary radar.

Significant research has been carried out to model accurately and with computationally efficient processing the RCS and Doppler signatures of wind turbines [8-10]. The use of scaled models of realistic turbines for controlled measurements in laboratory has also been reported [11-12], showing the effect of different rotation speeds and yaw angles on the micro-Doppler signatures and analysing the statistics of such signatures as they fluctuate. The impact of wind farm clutter on real radar systems and their performance has been also investigated, for instance on Ground Moving Target Indication (GMTI) for targets within the wind turbine area [13], on weather radar stations [14], on maritime radar systems [15], and on the detection and tracking capabilities of unauthorized aircraft entering a restricted zone [16]. Novel wind turbine designs have been proposed to replace the common three-bladed horizontal axis turbines, such as vertical axis turbines, simulated and tested with a scaled model

in [17], and wind lens prototypes have been developed and measured experimentally in [18]. The use of partial reshaping of the nacelle together with RAM to reduce the overall RCS of turbines has been considered in [19], also evaluating the increased cost due to the absorbing material on the blades, whereas in [20] the integration of RAM and lighting protection systems is discussed through numerical simulations that model the application of the absorber onto different sections and areas of the blades. Additional digital signal processing algorithms have been proposed to mitigate the effects of wind farm clutter on radar signals and their performance [21-22]. Bistatic and multistatic radar systems have also been mentioned as a solution to address the wind farm clutter issue [7]. By exploiting multistatic geometries, these systems may offer additional degrees of freedom over conventional monostatic radar and can potentially provide advantages in dealing with wind farm clutter, such as a lower Doppler spread, multi-perspective information on targets, and lower radar clutter-to-target cross section.

In general little information has been published on actual experiments involving operating wind farms and radar systems. A comprehensive experimental campaign aimed at characterizing the monostatic RCS and Doppler signature of a wind farm at four radar bands, namely L, S, C and X, was performed in the past by the US Air Force Research Laboratory [23-24]. The experimental data collected showed very good agreement with the data generated through numerical simulations using an accurate CAD model of the turbines. In [25] the authors show additional experimental data with wind turbine signatures recorded by a weather surveillance Doppler radar, and present interpolation techniques to mask the clutter at the expense of spatial resolution.

To the best of our knowledge very little prior literature exists on experimental multistatic wind farm clutter. In this paper we show simultaneous monostatic and bistatic signatures of operational wind turbines as collected in May 2015 with an S-band pulsed radar and an X-band CW radar, developed respectively at University College London and Cranfield University, Shrivenham. For each recording, the possibility of comparing simultaneous monostatic and bistatic signatures with two different bistatic angles, and simultaneous multiband signatures makes these data significantly novel. Preliminary data collected in January 2015 were shown in our previous work in [26] where an empirical comparison between monostatic and bistatic data at narrow bistatic angle (approximately 6.5°) was presented. This paper expands the past work analysing a new set of data collected with wider bistatic angles (13° up to 23°) to characterize the wind turbine clutter as function of such angle. More radar nodes were also deployed for this experiment, namely three rather than two at S-band and two rather than one at X-band, allowing further comparisons between datasets. Some quantitative parameters such as the overall Doppler bandwidth and the average Doppler power across ranges of Doppler bins have also been extracted in this study for a more quantitative comparison of monostatic vs bistatic data.

This paper is organised as follows. Section 2 presents the experimental setup of the measurements and the two radar systems used to collect the data. Section 3 describes the analysis of the data with a comparison of monostatic ad simultaneous bistatic spectrograms obtained at different polarizations and bistatic angles, as well as at both S-band and X-band. Section 4 concludes the paper and discusses future work.

2. Radar systems and measurement setup

The data analysed in this work have been collected using two radar systems in a joint experiment between University College London and Cranfield University. The first system is the S-band multistatic pulsed coherent system NetRAD. NetRAD has been developed over a number of years at University College London [27] and has provided novel results in different research fields such as sea clutter characterisation and human micro-Doppler [28-30]. NetRAD has three distinct but essentially identical nodes, one of which is used as a monostatic transceiver (node 3) and the other two as receive-only nodes (node 1 and node 2). For this work, the transmitted power was 200 mW, the frequency 2.4 GHz, the pulse length 0.6 μs, the bandwidth of the linear chirp that modulates the pulse 45 MHz, the pulse repetition frequency (PRF) 5 kHz, and the length of each recording 10 s. Three identical antennas with a 10° x 10° beam-width and a 24 dBi gain were deployed. The second radar system is the Cranfield University X-band continuous wave (CW) radar. The radar consists of two nodes which transmit approximately 15 dBm each at a frequency close to 10 GHz. Each node provides the in-phase (I) and quadrature (Q) components of the received signal, and is composed of two identical horn antennas which for these experiments were separated of about 25 cm. The gain of the antennas was approximately 20 dB at both nodes, and the antenna beam-width was 15° x 20° at Node 3 and 11.5° x 15.5° at Node 2. The I component and the Q component of the target echoes were low-pass filtered and then digitised with a TiPie HS4 oscilloscope at a sampling rate of 10 kHz and with a 12-bit resolution.

Fig. 1 shows a sketch of the experimental setup and the deployment of the radar systems. The experiment took place at the Westmill Wind Farm in Watchfield, near Swindon, in May 2015. This wind farm consists of five 49 m tall wind turbines each one carrying three 31 m long blades. Only the two turbines closest to the radar nodes were used as targets, as shown in the sketch in Fig. 1. A top view of the wind farm is also provided in Fig. 1 for completeness, highlighting the position of two S-band nodes and their antenna beams when pointing at the first turbine under test. The average wind speed during the experiment was estimated between 12 m/s and 17 m/s as from historical data of the nearest weather station. The three NetRAD nodes were separated by 50 m and provided monostatic and bistatic data with two different bistatic angles β for each measurement. Two monostatic X-band

radar were deployed at the location of the monostatic S-band node and at the farthest bistatic S-band node to provide comparative data. It should be noted that the monostatic and bistatic S-band data were collected simultaneously as the three nodes are synchronised by a common clock and trigger. The X-band data were also collected simultaneously with the S-band data, apart from a small delay of fractions of second due to non-perfect manual synchronisation of the starting time of both radar systems. The difference in start times of the systems was negligible in the later processing, as multiple rotations of the turbine were included in both datasets allowing the average behaviour to be characterised sufficiently for direct comparisons between the two systems. The distance of the first and second turbine under test (TUT1 and TUT2 respectively) from the baseline was approximately 246 m and 439 m. The resulting bistatic angles for TUT1 and TUT2 are respectively 23° and 13° considering the farthest bistatic node (node 2), and approximately 11.5° and 6.5° considering the nearest bistatic node (node 1).

It should be noted that the data collected are in the near field of the wind turbine. The minimum far-field distance required for this kind of measurements considering the 12.5 cm wavelength at S-band and the 31 m blade length of the turbine would be in the range of 15 km according to the usual relation $2D^2/\lambda$ for far-field. The far-field distance is actually even longer if the calculation is repeated for X-band (approximately 64 km) or if the whole tower height is considered and not only the blade, making far-field measurements infeasible in practice with any research radar at microwave frequencies. In [11] and [31] this issue is also discussed and it is argued that it is not unlikely that wind farms, especially those with the largest turbines, are located in the near-field of radar systems and hence the experimental analysis of near field data is still very valuable.

Separate datasets were collected for the TUT1 and the TUT2 repointing the antennas to the nacelle of the particular turbine under test using optical alignment via rifle-scopes. The data collected for different turbines are therefore not simultaneous. Data at different polarizations were collected for both turbines, namely VV (vertical transmitted and vertical received) and HH (horizontal transmitted and horizontal received) data. The change of polarization required to manually rotate the antennas, therefore VV and HH data are not simultaneous even if referring to the same turbine under test.

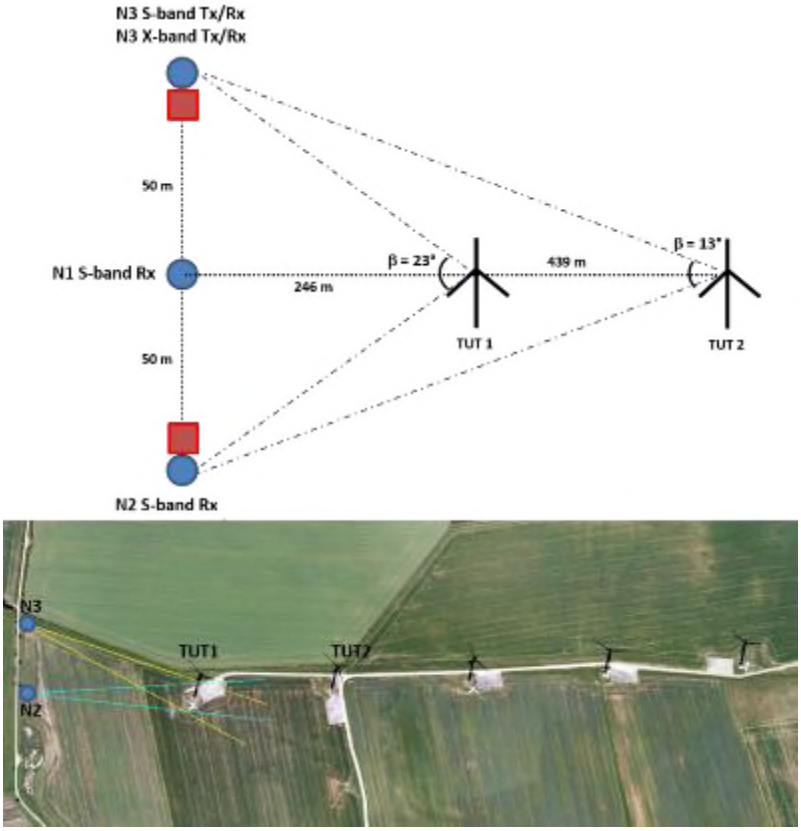

Figure 1 Sketch and top view of the experimental setup with S-band and X-band radar deployed and the turbines

3. Data Analysis

The resolution for S-band data is sufficient to discriminate in range the return from different turbines, hence only the signal at the range bin where the turbine return is present was used for Doppler processing. As an example, Fig. 2 shows two Range-Time-Intensity (RTI) plots for monostatic and bistatic data collected at node 3 and node 2, respectively, when measuring the returns of the TUT1. The return of the particular turbine of interest can be identified as a vertical line in these plots and used for the Doppler analysis in this section.

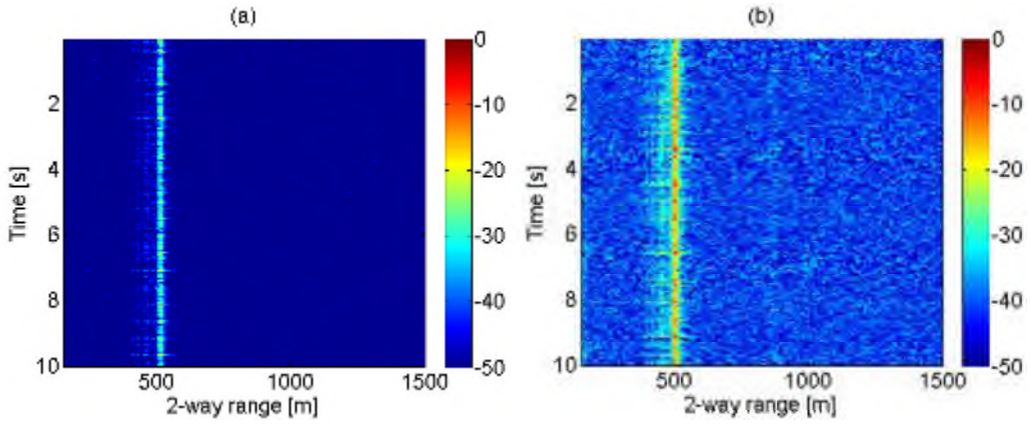

Figure 2 RTI plots for monostatic (a) and bistatic (b) VV polarised data collected for TUT1

The CW radar at X-band has no range resolution, so the return from all the turbines detected by the radar will contribute to the Doppler signature. The Doppler processing used Short Time Fourier Transform (STFT) with 0.6 s Hamming window at S-band and about $1/4^{th}$ at X-band, and 95% overlap to produce spectrograms. These spectrograms are shown in this section with the goal of characterizing monostatic vs bistatic wind turbine signatures, and investigating whether bistatic data can help mitigate wind farm clutter.

3.1 S-band data

Fig.3-Fig.5 show the monostatic and bistatic signatures of the measured wind turbines, in the form of a spectrogram, at different polarizations. For the VV polarized data in Fig.3 and Fig.4 it is possible to observe that the overall bandwidth of the Doppler signature appears to decrease from monostatic to bistatic data, and this effect is more visible for the data collected with a wider bistatic angle (i.e. at node 2 in comparison with node 1). In the VV data this effect appears to be more significant for data referring to the TUT1 compared with the TUT2, and this may be related to the different aspect angles that the two turbines present between the rotation plane of the blades and the line of sight of the radar, as well as to the different bistatic angles related to the TUT1 and the TUT2. The positive blade flash appears to be more intense than the negative flash for data at node 3 and node 1 (monostatic and bistatic with narrower bistatic angle respectively). This was already observed in the analysis of previous data with narrower bistatic angles [26], although it should be noted that the orientation of the turbines may have been different for the current and older datasets as they were recorded at different times. On the contrary the negative Doppler flashes appear more intense relatively to the strongest components in Fig. 3b and 4b, showing that at increased bistatic angle the wind turbine signature can be significantly different. In Fig. 3c and 4c the micro-Doppler signatures exhibit an additional, faint contribution at Doppler values higher than the main blade flashes, at approximately 750-900 Hz. This may be related to blade-tower-blade multi-bounce scattering phenomena, as highlighted in [24], where similar contributions in their experimental monostatic spectrograms can be observed. The decreasing overall Doppler bandwidth of the signature from monostatic to bistatic data can be also seen for HH data in Fig. 5. In these data the negative blade flashes appear more intense than the positive ones for both monostatic and bistatic data. As for the VV data, this seems to confirm the empirical observations for previous data at narrower bistatic angles [26], although it should be noted that the orientation of the turbine may have been different in the two datasets. The faint vertical lines in Fig. 5b are artefacts caused by the imperfect phase synchronization between the transmitter node and the receivers (and they appear only on HH polarised data collected at bistatic nodes 1 and 2). They are not thought to be related to the actual turbine signature. The Doppler shift of the signatures appears to have far larger values than those directly related to the average wind speed recorded at the nearest weather station, i.e.

between 12 m/s and 17 m/s which correspond to Doppler shifts of 192 Hz and 272 Hz, respectively. This discrepancy is believed to be related to the difference between the wind speed recorded at the weather station and the actual wind speed at the turbine blades, as well as to the uncertainty on the relation linking the actual rotation speed induced by the wind and the wind speed (which depends on the way the particular model of turbine works and cannot be estimated from the radar data).

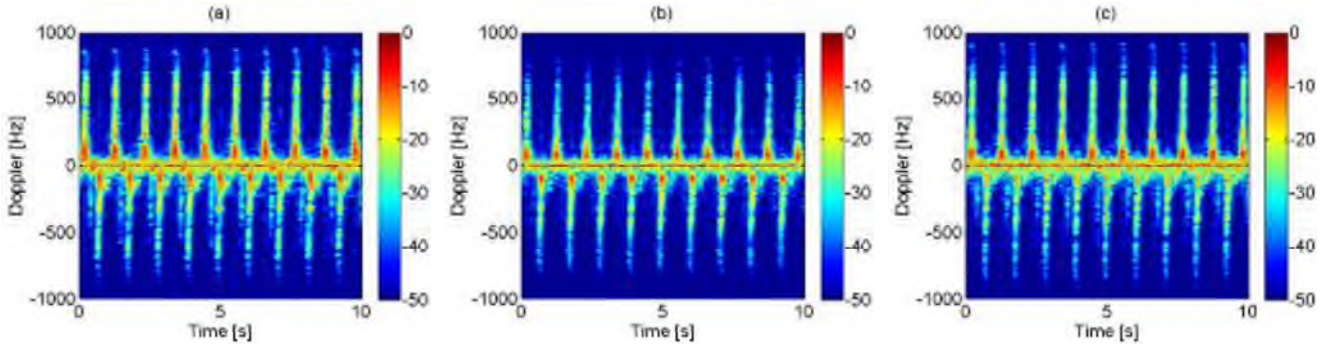

Figure 3 NetRAD spectrograms for TUT1 and VV polarization: (a) node 1 data, (b) node 2 data, and (c) node 3 data

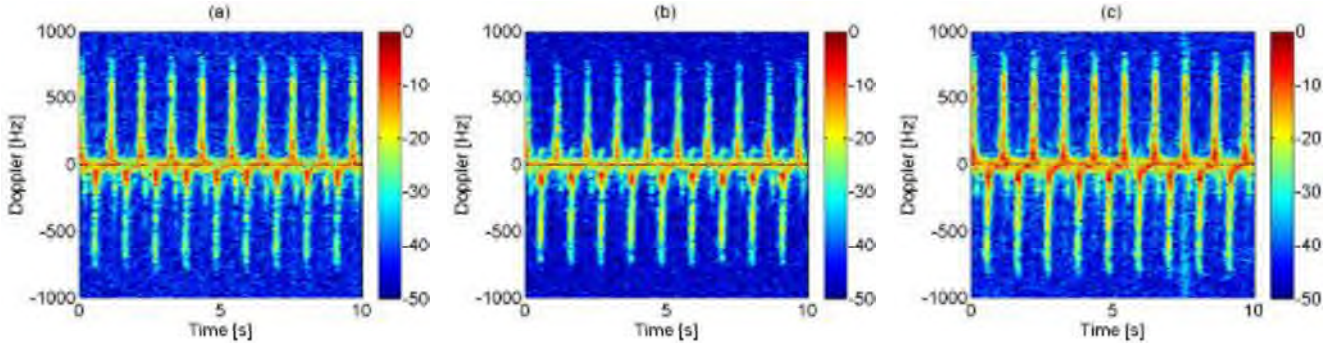

Figure 4 NetRAD spectrograms for TUT2 and VV polarization: (a) node 1 data, (b) node 2 data, and (c) node 3 data

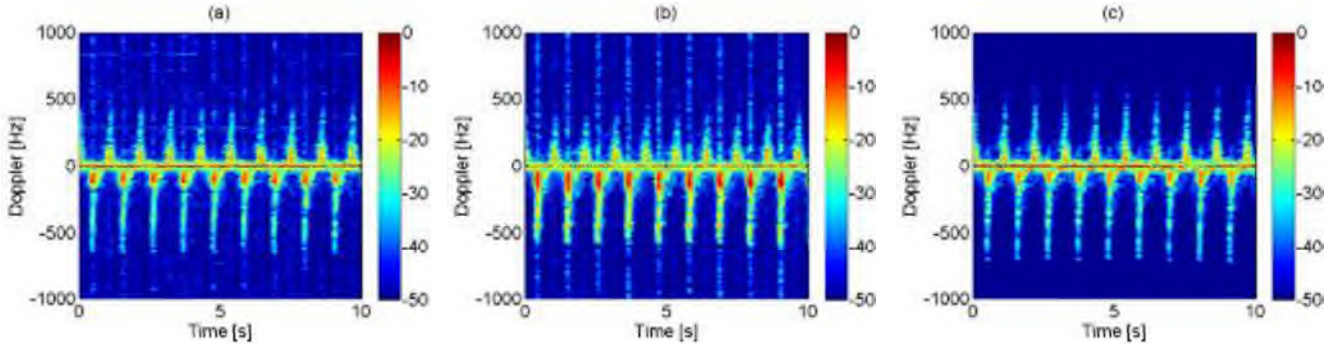

Figure 5 NetRAD spectrograms for TUT1 and HH polarization: (a) node 1 data, (b) node 2 data, and (c) node 3 data

Rather than simply making qualitative comparisons between the spectrograms, specific parameters can be extracted for a more quantitative comparison of the monostatic and bistatic wind turbine signatures. The Doppler centroid and bandwidth centroid of the wind turbine signatures have been calculated as in equations (1) and (2) where f_C is the Doppler centroid, B_C the Bandwidth centroid, $S(i,j)$ the spectrogram at the i^{th} Doppler bin and j^{th} time bin. The Doppler centroid is an estimate of the centre of gravity of the turbine micro-Doppler signature, and the Doppler bandwidth provides an estimate of the

signature bandwidth around the Doppler centroid [18]. The advantage of these estimators is that they are independent of any normalisation and hence can be applied without loss of information to non-calibrated data.

$$f_c(j) = \frac{\sum_i f(i)S(i,j)}{\sum_i S(i,j)} \quad (1)$$

$$B_c(j) = \sqrt{\frac{\sum_i (f(i)-f_c(j))^2 S(i,j)}{\sum_i S(i,j)}} \quad (2)$$

Fig. 6 and 7 show a comparison between the Doppler centroid and bandwidth relative to the monostatic and bistatic data, for both the VV and HH polarisations. The Doppler centroid of the monostatic data appears to have higher positive peak values than that of the bistatic data for both polarisations. The Doppler bandwidth appears to be on the average higher for the monostatic data in comparison with bistatic data in HH polarisation and for the TUT2 in VV polarisation (Fig. 6d), whereas the opposite result is obtained for the TUT1 in VV polarisation (Fig. 6b). These results appear not to provide a clear and unambiguous conclusion, as in VV polarisation and bistatic angle 23° (Fig. 6b) the bandwidth of the clutter signature is more significant for the bistatic case, whereas in VV polarisation with bistatic angle 13° (Fig. 6a) and in HH polarisations (Fig. 7b and 7d) the bandwidth of the clutter signature is more spread for the monostatic case.

Results from the analysis of additional datasets collected on the same day are also shown in Fig. 8 and Fig. 9, for VV polarised and HH polarised data, respectively. The positive peaks of the Doppler centroid appear to be higher for the monostatic data for VV polarisation (Fig. 8a and 8c) and for HH polarised data for the TUT 2 (Fig. 9c). The Doppler bandwidth shows similar trends as observed in Fig. 6 and 7 with values on average higher for the monostatic data in HH polarised data (Fig. 9b and 9d) and VV polarised data for the TUT2 (Fig. 8d), but higher for the bistatic VV polarised data for the TUT1 (Fig. 8b).

These results seem to suggest that the choice of polarisation, the deployment geometry of the nodes (hence bistatic angles), and the angle between the line-of-sight of the radar and the rotation plane of the turbine blades can all have an impact on the clutter affecting radar nodes. The radar operator can potentially choose suitable bistatic angles when deploying multiple radar nodes, but the effect of the aspect angle between the radar line-of-sight and the yaw axis of the turbine cannot be controlled as it changes dynamically with wind speed and direction. It is potentially expected that the clutter micro-Doppler signature is less spread out in Doppler at some nodes of multistatic radar or of systems with multiple independent nodes, and hence less detrimental to the performance of the radar (for instance as

in Fig. 7b, 7d, and 9d). However further work is required to characterize and quantify more accurately the behaviour of the clutter as a function of the aforementioned parameters and the potential advantages of bistatic/multistatic configuration.

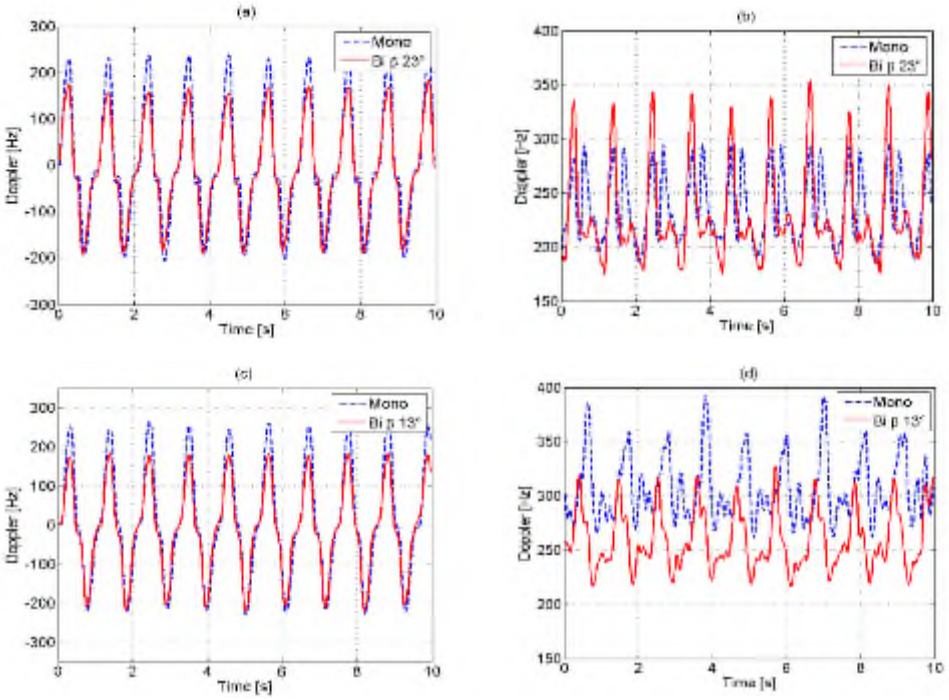

Figure 6 Comparison monostatic vs bistatic VV polarised data for Doppler centroid (a) and Bandwidth centroid (b) for TUT1, and Doppler centroid (c) and Bandwidth centroid (d) for TUT2

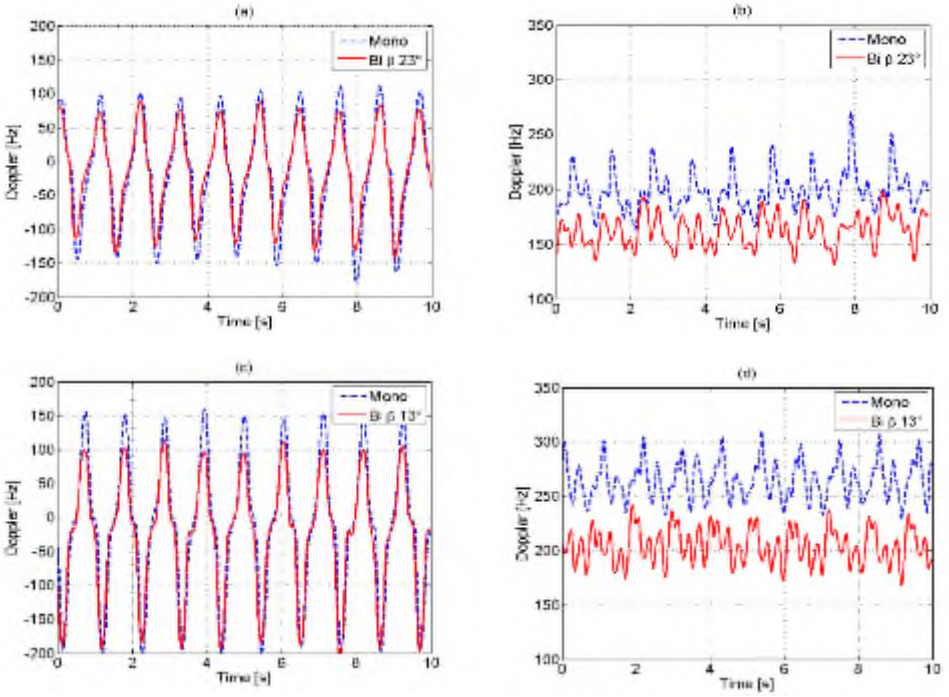

Figure 7 Comparison monostatic vs bistatic HH polarised data for Doppler centroid (a) and Bandwidth centroid (b) for TUT1, and Doppler centroid (c) and Bandwidth centroid (d) for TUT2

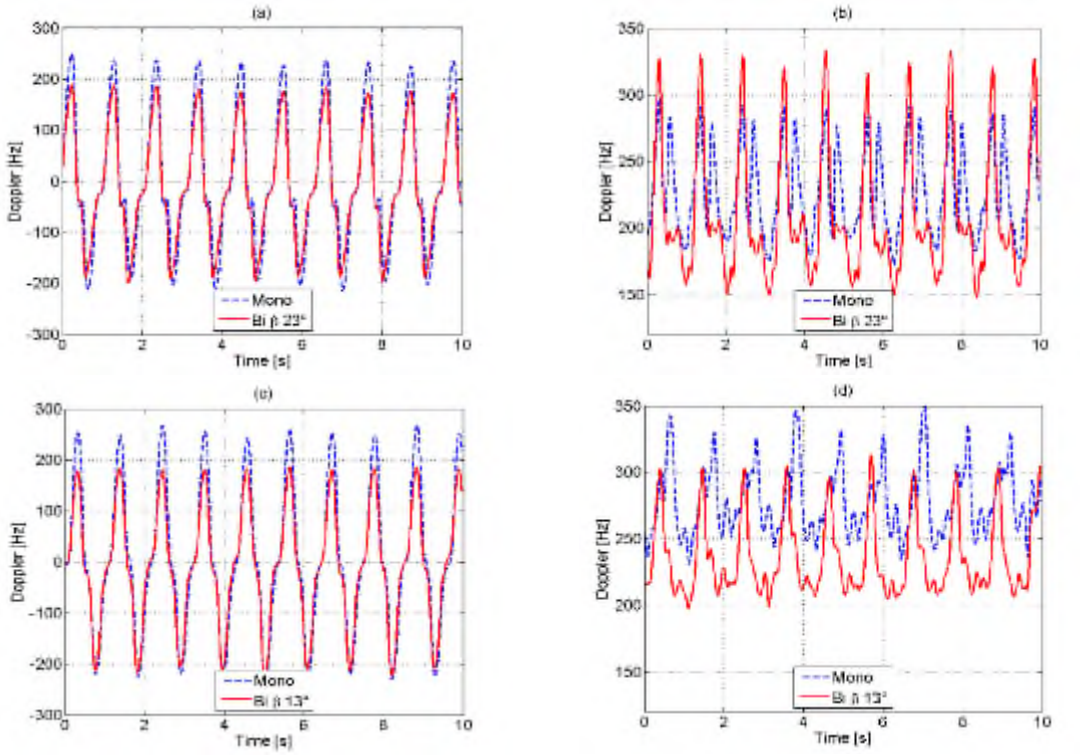

Figure 8 Comparison monostatic vs bistatic VV polarised additional data for Doppler centroid (a) and Bandwidth centroid (b) for TUT1, and Doppler centroid (c) and Bandwidth centroid (d) for TUT2

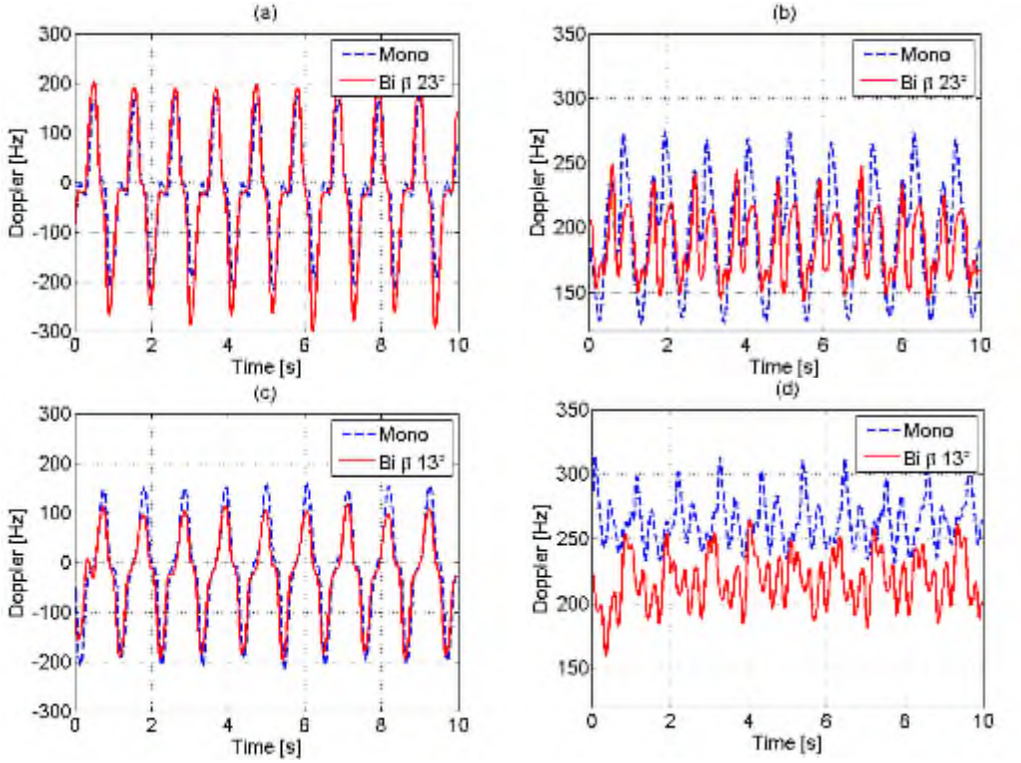

Figure 9 Comparison monostatic vs bistatic HH polarised additional data for Doppler centroid (a) and Bandwidth centroid (b) for TUT1, and Doppler centroid (c) and Bandwidth centroid (d) for TUT2

Another parameter to consider for a monostatic vs bistatic quantitative comparison is the average intensity of the micro-Doppler signature associated to the blade flashes across a set of predefined Doppler bins. Fig. 10 shows examples of these comparisons for VV polarized data and for both TUT1 and TUT2. Two intervals of Doppler bins have been considered, namely 200-300 Hz and 600-700 Hz. The peak of the monostatic average micro-Doppler intensity appears to be approximately between 3 and 4 dB higher than the bistatic one at lower Doppler bins (200-300 Hz), whereas at higher Doppler bins (600-700 Hz) the difference is more significant, approximately 6 to 8 dB.

Tables 1 and 2 summarize the values of the micro-Doppler intensity averaged across the whole duration of the spectrogram for different 100 Hz wide Doppler intervals covering the entire bandwidth, respectively for VV and HH data. Results for both TUT1 and TUT2 with the time of the measurements are reported, as well as the difference between the monostatic and bistatic result for comparison. It should be noted that there was no turbine signature recorded at Doppler bins higher than 400 Hz for the TUT1 at HH polarizations, hence some fields in the table are left empty. For the VV data the monostatic intensity appears to be in general higher than the bistatic at positive Doppler bins, with differences up to approximately 8 dB. This seems to suggest that the bistatic turbine signature is less intense than the monostatic with the reasonable assumption that the radar nodes are identical. The situation is different at the negative Doppler bins where the results do not show a clear trend and the bistatic signature appears more intense at Doppler bins between -200 Hz and -600 Hz, and then less intense than the monostatic at Doppler bins between -600 Hz and -900 Hz. For HH data there is again a mixed trend, as the monostatic intensity appears to be lower than the bistatic at negative Doppler bins for both TUT1 and TUT2, whereas at positive Doppler bins the bistatic intensity is lower for the TUT1 (wider bistatic angle).

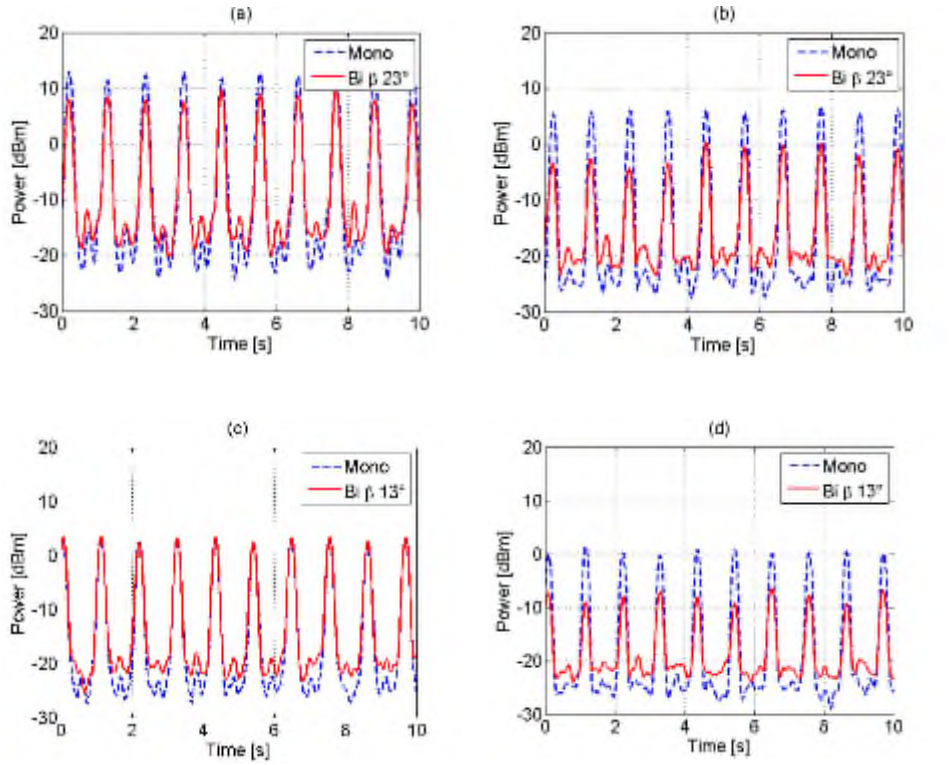

Figure 10 Comparison of average micro-Doppler intensity for monostatic and bistatic VV polarised data: (a) average across 200-300 Hz for TUT1, (b) average across 600-700 Hz for TUT1, (c) average across 200-300 Hz for TUT2, and (d) average across 600-700 Hz for TUT2

Table 1 Comparison of peak of the average micro-Doppler intensity across Doppler bins of wind turbines signature for VV polarized monostatic vs bistatic data

	VV data - TUT1 – 11:10:02 – β=23°			**VV data - TUT2 – 11:32:02 - β=13°**		
Doppler bins [Hz]	**Avg Intensity Mono [dBm]**	**Avg Intensity Bi [dBm]**	**Diff mono and bi**	**Avg Intensity Mono [dBm]**	**Avg Intensity Bi [dBm]**	**Diff mono and bi**
200-300	12.42	8.43	4.00	2.83	3.08	-0.25
300-400	7.29	7.74	-0.45	1.47	-0.55	2.02
400-500	8.95	4.72	4.23	2.46	0.35	2.12
500-600	7.87	2.76	5.11	3.15	-3.78	6.93
600-700	5.97	-1.69	7.66	0.35	-7.91	8.26
700-800	-3.82	-10.89	7.07	-9.60	-11.15	1.55
800-900	-9.63	-15.82	6.19	-15.71	-20.81	5.10
-300 -200	8.28	10.59	-2.31	0.68	-0.16	0.83
-400 -300	6.94	9.52	-2.58	-0.03	2.26	-2.29
-500 -400	5.18	9.26	-4.08	-2.20	4.09	-6.28
-600 -500	-0.93	0.02	-0.95	-4.53	2.02	-6.55
-700 -600	-1.37	-2.63	1.26	-4.95	-3.26	-1.69
-800 -700	-4.98	-5.13	0.15	-8.28	-8.26	-0.03
-900 -800	-9.85	-17.22	7.37	-17.76	-20.62	2.86

Table 2 Comparison of peak of the average micro-Doppler intensity across Doppler bins of wind turbines signature for HH polarized monostatic vs bistatic data

	HH - TUT1 – 12:03:20 - β=23°			**HH - TUT2 – 12:16:32 - β=13°**		
Doppler bins [Hz]	**Avg Intensity Mono [dBm]**	**Avg Intensity Bi [dBm]**	**Diff mono and bi**	**Avg Intensity Mono [dBm]**	**Avg Intensity Bi [dBm]**	**Diff mono and bi**
200-300	2.69	0.18	2.51	-5.83	-2.11	-3.73
300-400	0.11	-4.30	4.42	-6.31	-3.39	-2.92
400-500	-	-	-	-11.23	-9.79	-1.44
500-600	-	-	-	-10.48	-12.88	2.40
-300 -200	6.27	10.96	-4.69	-4.86	-1.23	-3.64
-400 -300	2.38	8.53	-6.15	-5.61	-0.61	-4.99
-500 -400	3.82	13.75	-9.93	-5.62	-2.68	-2.95
-600 -500	0.08	7.50	-7.42	-8.80	2.17	-10.97
-700 -600	-	-	-	-6.72	0.01	-6.73

3.2 X-band data

The X-band data were collected using two identical monostatic CW radar systems which were deployed at Node 2 and Node 3, as shown in Fig. 1. Fig. 11 presents examples of spectrograms for both VV polarised and HH polarised data which were collected simultaneously to the S-band data shown in Fig. 3 and Fig. 5. These were calculated using the same window overlap as for the S-band data (95%) and a quarter of the window length (0.15 s) in order to allow a comparison, with the same Doppler shift to frequency resolution ratio, between the S-band and X-band data. Results show that the micro-Doppler signature of the turbine is spread across a wider range of Doppler frequencies which is, as expected, approximately four times broader than that of the S-band data (being the X-band carrier frequency roughly four times higher). The signature at node 2 shows a lower Doppler spread in both VV and HH polarisations. Although each X-band node worked as independent monostatic node, these results seem to show that multiple nodes surveying an area from different spatial locations can be affected differently by wind farm clutter depending on polarisations and aspect angle between node and yaw axis of the turbine. In the previous section similar effects were observed for S-band monostatic vs bistatic data, i.e. the possibility that one radar node is affected by more favourable clutter when multi-perspective views from multiple nodes are used. The contribution of the blade components moving away from the radar generate a stronger return in HH polarisation as for the S-band data. For both polarisations the blade flashes reach higher negative Doppler shifts.

The Doppler and bandwidth centroid parameters were also estimated for the X-band data in order to allow a quantitative comparison. Fig. 12 shows the Doppler bandwidth and Doppler centroid relative to the spectrograms of Fig. 11. Results show that the Doppler centroid for VV polarised data presents higher positive and negative peaks at Node 3 (Fig. 12a) and that the Doppler bandwidth is also larger

for the node 3 data (Fig. 12b) corroborating the empirical results from the spectrograms. For the HH polarised data the situation is reversed and higher values of the two parameters are visible for node 2 data. The Doppler centroid in Fig. 12c reaches higher values and exhibits a larger Doppler bandwidth in Fig. 12d as a results of the strong return of the blade for negative Doppler values at about -1 kHz. At the time of the measurements the two X-band nodes were not perfectly synchronised hence the time delay between the Doppler centroid peaks at node 3 and node 2 in some of the data.

Fig. 13 shows the average Doppler power across Doppler bins at X-band for the VV data relative to the S-band measurements in Fig. 10. The average Doppler power was calculated for two different ranges of frequencies, 800-1200 Hz and 2400-2800 Hz. Although the CW radar does not separate the contribution of each turbine, the X-band antennas were aligned to steer alternatively at the TUT1 and at the TUT2 to collect the data used in Fig. 13. The range of Doppler bins considered was scaled by a factor of four switching from S-band to X-band. Results show that the peaks of the average power appear to be approximately 10 dB higher for data recorded at node 2 in the range 800-1200 Hz, whereas the difference reduces to a couple of dB in the range 2400-2800 Hz.

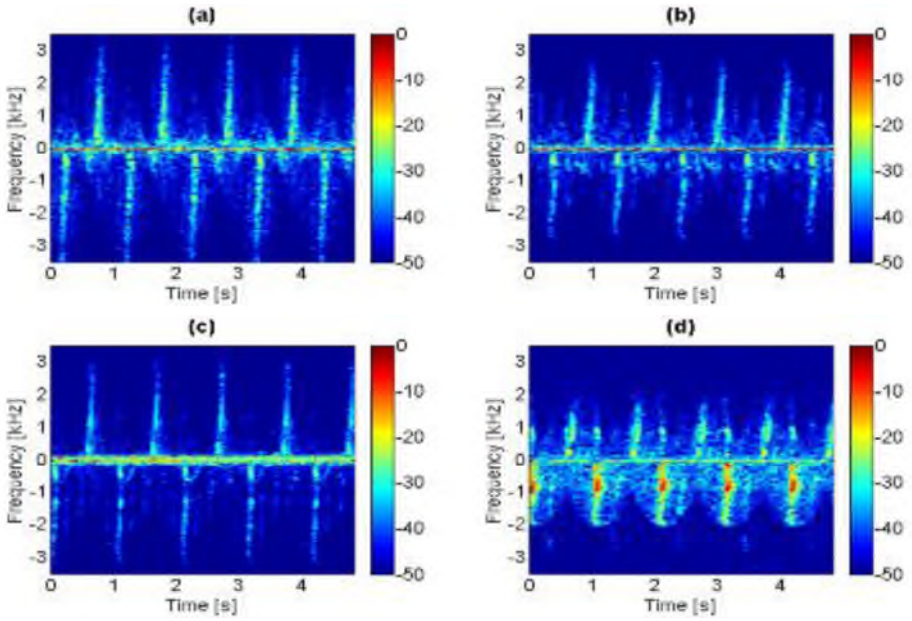

Figure 11 X-band spectrograms for TUT 1 at VV polarization for node 3 (a) and node 2 (b), and at HH polarization for node 3 (c) and node 2 (d)

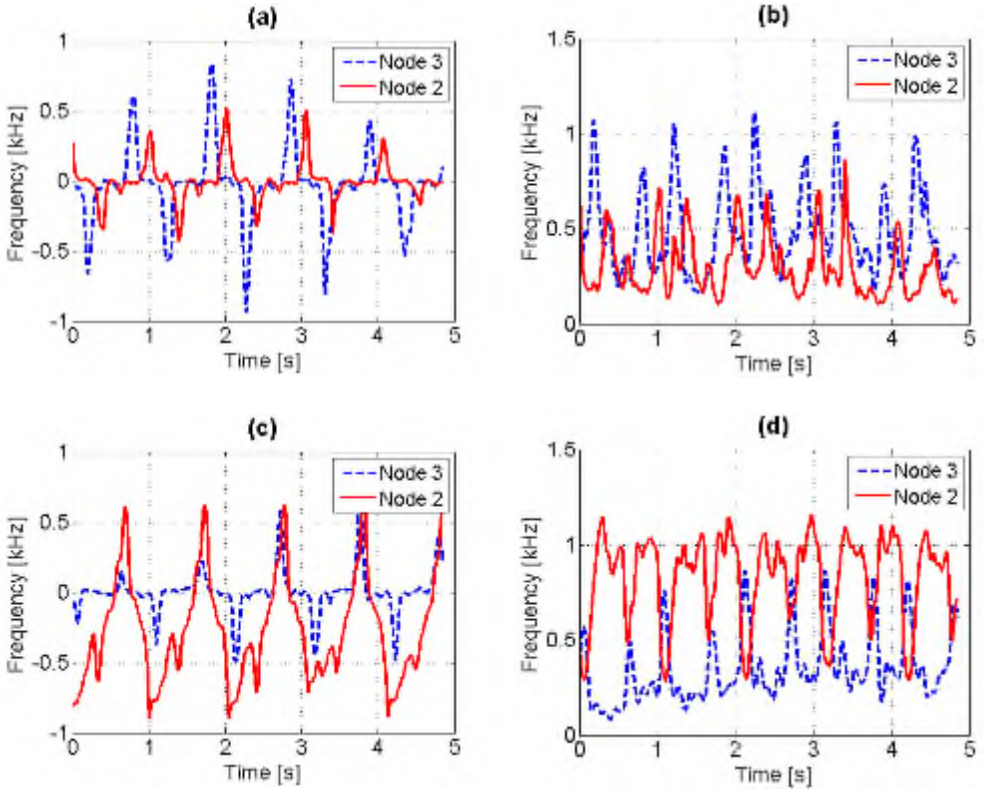

Figure 12 Doppler centroid (a) and bandwidth centroid (b) for X-band radar nodes at VV polarization, and Doppler centroid (c) and bandwidth centroid (d) for X-band radar nodes at HH polarization

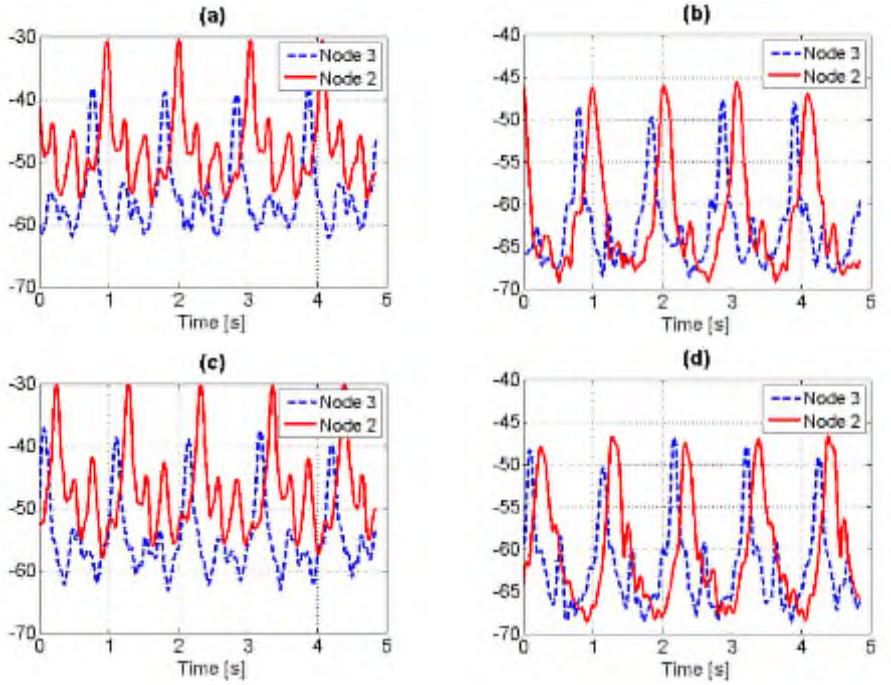

Figure 13 Comparison of average Doppler for node 3 and node 2 X-band VV polarised data: (a) average across 800-1200 Hz for radar steering at TUT1, (b) average across 2400-2800 Hz for radar steering at TUT1, (c) average across 800-1200 Hz for radar steering at TUT2, and (d) average across 2400-2800 Hz for radar steering at TUT2

4. Conclusion

This paper presents experimental micro-Doppler signatures from simultaneous monostatic and bistatic measurements of operational wind turbines. The data were collected in May 2015 using the UCL multistatic S-band radar system NetRAD and the Cranfield University X-band radar system, providing a multiband dataset with bistatic angle up to 23° with both VV and HH polarizations. Such data are expected to be significantly novel as multistatic multiband measurements of wind turbine signatures have not been reported before to the best of our knowledge.

Monostatic and bistatic spectrograms from several measurements have been presented and their key differences have been described empirically and through numerical parameters. The analysis of the micro-Doppler signatures and of quantitative parameters, such as Doppler centroid and bandwidth, has shown that wind turbine clutter signatures are affected by the choice of polarisation, by deployment geometries of the radar nodes and the resulting bistatic angles, and by the aspect angle between the radar line-of-sight and the yaw axis of the turbines. Depending on the aforementioned parameters, in some cases Doppler centroid peaks and average values of Doppler bandwidth for the S-band data appear to be lower at the bistatic node, in other cases at the monostatic node. Similar results are obtained for the X-band data, where the two radar nodes were working as independent monostatic nodes, but co-located with the S-band monostatic and bistatic nodes, hence exploiting spatial diversity.

One of the limitations of the available data is the difficulty of estimating the aspect angle between the blade rotation plane and the line of sight of the radar, as the orientation of the turbine changes constantly to adapt to the changing wind direction. This aspect angle has a direct impact on the micro-Doppler signature and characterizing its effect combined with the effect of different bistatic geometries and polarisations requires further experimentation, in order to identify the best configurations of the radar nodes to minimize the impact of wind farm clutter.

However, since there is little evidence in the literature of experimental data of operational wind turbines at two different bands and with simultaneous recording of monostatic and bistatic data, it is believed that the results presented here can help better characterise and understand wind farm clutter. The results appear to show that in some conditions the clutter signature is less spread out with lower values of Doppler centroid and bandwidth at one of the nodes, which could be advantageous for target detection in the Doppler domain where possible targets of interest (for instance small aircraft or helicopters) may exhibit Doppler shifts comparable to those generated by the wind farm. In that case tasks such as target detection and classification are expected to be more easily performed exploiting the information from the node less affected by wind farm clutter, whereas the overall performance of

the radar system could be severely hindered in case of single node systems when the clutter is particularly detrimental to that node.

A better understanding of the complex, non-stationary micro-Doppler signature of wind farm clutter that these results contribute to is expected to help improve more effective solutions to mitigate and filter the clutter, and further work will be carried out with this aim. This will include the collection of more data at different bistatic angle and geometries, and different environmental conditions (wind speed, direction, and turbine orientation) to move towards a statistical characterization of multistatic wind turbine clutter that takes into account all the variables involved. Another possible option is using a realistic scaled model of the turbine for laboratory measurements where rotation speed and orientation of the turbine can be varied in a controlled manner and then comparing the results to the actual experimental data on the operational turbine on site. The actual effect of monostatic vs bistatic wind turbine clutter on target detection in the Doppler domain can also be investigated embedding different simulated target signatures and trajectories into the experimentally measured wind turbine signatures.

Acknowledgement

The authors are grateful to the IET for the A F Harvey Prize 2013 awarded to Prof Hugh Griffiths which partially funds this work.

References

[1] "The EU's Target for Renewable Energy: 20% by 2020", *Volume I: Report, Authority of the House of Lords*, 24/10/2008.

[2] http://www.renewableuk.com/en/renewable-energy/wind-energy/onshore-wind/index.cfm, Accessed 21/08/2015.

[3] http://www.renewableuk.com/en/our-work/aviation-and-radar/index.cfm, Accessed 21/08/2015.

[4] https://www.gov.uk/onshore-wind-part-of-the-uks-energy-mix#wind-turbines-aviation-and-radar, Accessed 21/08/2015.

[5] C. A. Jackson, "Windfarm characteristics and their effect on radar systems," *2007 IET International Conference on Radar Systems*, pp. 1-6, 15-18 October, Edinburgh, UK.

[6] C. A. Jackson and M. M. Butler, "Options for mitigation of the effects of windfarms on radar sytems," *2007 IET International Conference on Radar Systems*, pp. 1-6, 15-18 October, Edinburgh, UK.

[7] Civil Aviation Publication CAP 670, 'Air Traffic Service (ATS) Safety Requirements', available online and accessed 10/02/2016, Part C, Section 3, Appendix A, pp. 1-63.

[8] Y. F. Lok, A. Palevsky, and W. Jian, "Simulation of radar signal on wind turbine," *IEEE Aerospace and Electronic Systems Magazine*, vol. 26, pp. 39-42, 2011.

[9] L. R. Danoon and A. K. Brown, "Modeling methodology for computing the radar cross section and Doppler signature of wind farms," *IEEE Transactions on Antennas and Propagation*, vol. 61, pp. 5166-5174, 2013.

[10] O. Karabayir, S. M. Yucedag, A. F. Coskun, O. M. Yucedag, H. A. Serim, and S. Kent, "Wind turbine signal modelling approach for pulse Doppler radars and applications," *IET Radar, Sonar & Navigation*, vol. 9, pp. 276-284, 2015.

[11] F. Kong, Y. Zhang, and R. D. Palmer, "Wind turbine radar interference studies by polarimetric measurements of a scaled model," *IEEE Transactions on Aerospace and Electronic Systems*, vol. 49, pp. 1589-1600, 2013.

[12] A. Naqvi, Y. Shang-Te, and L. Hao, "Investigation of Doppler features from wind turbine scattering," *IEEE Antennas and Wireless Propagation Letters*, vol. 9, pp. 485-488, 2010.

[13] S. Chiu and P. Beaulne, "Ground moving target indication inside a wind farm: interference and mitigation," *Proceedings of 10th European Conference on Synthetic Aperture Radar EUSAR*, 2014, pp. 1-4, 3-5 June, Berlin, Germany.

[14] F. Darcy and D. de la Vega, "A methodology for calculating the interference of wind farm on weather radar," in *Antennas & Propagation Conference LAPC 2009*, pp. 665-667, 16-17 November, Loughborough, UK.

[15] Olatz Grande, Josune Cañizo, Itziar Angulo, et al., "Simplified formulae for the estimation of offshore wind turbines clutter on marinerRadars," *The Scientific World Journal*, vol. 2014, Article ID 982508, 11 pages, 2014.

[16] A. F. Wind, J. D. Gerber, and J. D. Griesbach, "Impacts of wind turbine farm obscurations on aircraft escort probability of success," *2014 IEEE Radar Conference*, pp. 0603-0607, 19-23 May, Cincinnati, OH, USA.

[17] C. J. Li, R. Bhalla, and L. Hao, "Investigation of the dynamic radar signatures of a vertical-axis wind turbine," *IEEE Antennas and Wireless Propagation Letters*, vol. 14, pp. 763-766, 2015.

[18] A. Balleri, A. Al-Armaghany, H. Griffiths, K. Tong, T. Matsuura, T. Karasudani, et al., "Measurements and analysis of the radar signature of a new wind turbine design at X-band," *IET Radar, Sonar & Navigation*, vol. 7, pp. 170-177, 2013.

[19] J. Pinto, J. C. G. Matthews, and G. C. Sarno, "Stealth technology for wind turbines," *IET Radar, Sonar & Navigation*, vol. 4, pp. 126-133, 2010.

[20] L. Danoon, A. El-Makadema, and A. Brown, "On the integration of lightning protection with stealth coated wind turbine blades," *Wind Energy*, vol. 17, pp. 1577-1585, 2014.

[21] F. Nai, S. Torres, and R. Palmer, "On the mitigation of wind turbine clutter for weather radars using range-Doppler spectral processing," *IET Radar, Sonar & Navigation*, vol. 7, pp. 178-190, 2013.

[22] Gallardo-Hernando, B.; Pérez-Martínez, F.; Aguado-Encabo, F., "Detection and mitigation of wind turbine clutter in C-band meteorological radar," *IET Radar, Sonar & Navigation*, vol. 4, pp. 520-527, 2010.

[23] B. M. Kent, K. C. Hill, A. Buterbaugh, G. Zelinski, R. Hawley, L. Cravens, et al., "Dynamic Radar cross section and radar Doppler measurements of commercial General Electric windmill power turbines - Part 1: predicted and measured radar signatures," *IEEE Antennas and Propagation Magazine*, vol. 50, pp. 211-219, 2008.

[24] A. Buterbaugh, B. M. Kent, K. C. Hill, G. Zelinski, R. Hawley, L. Cravens, et al., "Dynamic radar cross section and radar Doppler measurements of commercial General Electric windmill power turbines - Part 2: predicted and measured Doppler signatures," *2007 Antenna Measurements Techniques Association (AMTA) Symposium*, St Louis, MO, USA.

[25] B. M. Isom, R. D. Palmer, G. S. Secrest, R. D. Rhoton, D. Saxion, T. L. Allmon, et al., "Detailed observations of wind turbine clutter with scanning weather radars," *Journal of Atmospheric and Oceanic Technology*, vol. 26, pp. 894-910, 2009/05/01 2009.

[26] M. Ritchie, F. Fioranelli, A. Balleri, and H. D. Griffiths., Measurement and analysis of multiband bistatic and monostatic radar signatures of wind turbines. *Electronics Letters*, 2015, v. 51, (14), p. 1112-1113.

[27] T. E. Derham, S. Doughty, K. Woodbridge, and C. J. Baker, "Design and evaluation of a low-cost multistatic netted radar system," *IET Radar, Sonar & Navigation*, vol. 1, pp. 362-368, 2007.

[28] W. A. Al-Ashwal, K. Woodbridge, and H. D. Griffiths, "Analysis of bistatic sea clutter - Part I: Average reflectivity," *IEEE Transactions on Aerospace and Electronic Systems*, vol. 50, pp. 1283-1292, 2014.

[29] W. A. Al-Ashwal, K. Woodbridge, and H. D. Griffiths, "Analysis of bistatic sea clutter - Part II: Amplitude statistics," *IEEE Transactions on Aerospace and Electronic Systems*, vol. 50, pp. 1293-1303, 2014.

[30] F. Fioranelli, M. Ritchie, and H. Griffiths, "Classification of unarmed/armed personnel using the NetRAD multistatic radar for micro-Doppler and Singular Value Decomposition features," *IEEE Geoscience and Remote Sensing Letters*, vol.12, no.9, pp.1933,1937, Sept. 2015.

[31] V. C. Chen, D. Tahmush, and W. J. Miceli, *Radar Micro-Doppler Signatures: Processing and Applications*, Chapter 12, pp. 345-381, *Institution of Engineering and Technology*, 2014.